Journal of Hazardous Materials 185 (2011) 958–969

Contents lists available at ScienceDirect

Journal of Hazardous Materials

journal homepage: www.elsevier.com/locate/jhazmat

Debromination of polybrominated diphenyl ethers by Ni/Fe bimetallic nanoparticles: Influencing factors, kinetics, and mechanism

Zhanqiang Fang*, Xinhong Qiu, Jinhong Chen, Xiuqi Qiu

School of Chemistry and Environment, South China Normal University, Guangzhou 510006, China

ARTICLE INFO

Article history:
Received 2 March 2010
Received in revised form 28 August 2010
Accepted 30 September 2010
Available online 8 October 2010

Keywords:
Ni/Fe bimetallic nanoparticles
Polybrominated diphenyl ethers
Debromination
Kinetics

ABSTRACT

Polybrominated diphenyl ethers have been identified as a new class of organic pollutants with ecological risk due to their toxicity, bioaccumulation, and global distribution. Proper remediation technologies are needed to remove them from the environment. In this paper, Ni/Fe bimetallic nanoparticles were synthesized by chemical deposition and used to degrade decabromodiphenyl ether (BDE209). The characteristics of Ni/Fe nanoparticles were analyzed by transmission electron microscopy, X-ray diffractometry, X-ray photoelectron spectroscopy, and Brunnaer–Emmett–Teller surface area analysis. Ni/Fe bimetallic nanoparticles with diameters in the order of 20–50 nm could effectively degrade BDE209 in the solvent (tetrahydrofuran/water). Influence factors, such as Ni/Fe nanoparticle dosage, initial BDE209 concentration, and Ni loading, on the removal of BDE209 were studied. The results indicated that the degradation of BDE209 followed pseudo-first-order kinetics, and the degradation rate of BDE209 increased with increasing the amount of nano Ni/Fe particles, Ni/Fe ratio, and decreasing the initial concentration of BDE209. Through analyzed the mass balance of the BDE209 removal, degradation was the main process of BDE209 removal. The mechanism of debromination was deduced by analyzing the reaction products using gas chromatography–mass spectrometry, the bromide ion in the solution and varying the solvent conditions. Stepwise hydrogen reduction is the main process of debromination, and the hydrion play an important role in the reaction. Moreover, the experiment of long term performance and leaching of Ni were also carried out to test the stability and durability of Ni/Fe nanoparticles in BDE209 degradation.

1. Introduction

Polybrominated diphenyl ethers (PBDEs) have been widely used as flame retardants in various industrial products, such as electronic equipment, furniture, and textile, in the past three decades [1]. According to literature [2], although some countries have limited the use of PBDEs in some aspects, the global demand for PBDEs is still large, especially in the case of decabromodiphenyl ether (BDE209). Due to their high hydrophobicity, persistence, and bioaccumulation, they have become ubiquitous in the environment [1–8] as well as in human and animal bodies [9–12]. The presence of PBDEs in the animal body has been found to affect the balance of thyroid and cause neurotoxicity [13]. The deca-BDE compound is classified by the US Environmental Protection Agency (EPA) as a possible human carcinogen [14]. Thus, finding a feasible way to eliminate PBDEs contamination has become a very urgent endeavor. Gerecke et al. [15] first described the microbial reductive debromination of BDE209 into lower mass PBDE congeners under anaerobic conditions. He et al. [16] and Robrock et al. [17] reported the microbial debromination of PBDEs and determined the debromination pathway. However, the biotic reductive debromination method was found to be inefficient, and further disposal strategies were needed. Recently, the application of photocatalysis technology has received attention worldwide. Photochemical debromination of PBDEs using ultraviolet light [18,19] and titanium dioxide [20] has been reported. Photocatalytic degradation can rapidly debrominate BDE209, but the requirement for UV light limits its engineering applications in environmental remediation [21].

Low cost zero-valent iron (ZVI) is known as a reducing agent for many halogenated organic compounds [22,23] including BDE209 [24]. The efficiency of ZVI in treating contaminants is highly dependent on the properties of the metal surface because the reduction reaction of contaminants mainly occurs on the surface of Fe. Nano zero-valent iron (NZVI) has been suggested to increase degradation efficiency due to its huge specific surface area. However, recent studies have proposed that NZVI has some shortcomings when used to reduce some halogenated organic compounds. For instance, the rate of dechlorination of polychlorinated biphenyls (PCBs) [23,25] is very low. In addition, the formation of iron oxide or hydroxide over the surface of NZVI [26] usually decreases their reactivity. In order to solve these problems, a second catalytic metal, such as Ni,

* Corresponding author. Tel.: +86 20 39310250; fax: +86 20 39310187.
E-mail address: lisan408@yahoo.cn (Z. Fang).

0304-3894/$ – see front matter © 2010 Elsevier B.V. All rights reserved.
doi:10.1016/j.jhazmat.2010.09.113

Cu, or Pd, has been incorporated with NZVI to form nano bimetallic particles [27]. In this system, Fe acts as an electron donor, and Ni, Cu, or Pd not only serves as a catalyst to enhance the rate of dehalogenation [28–30] but also prevents oxidation when the particles are exposed to air [26].

To date, Fe-based bimetallic nanoparticles have been widely used to degrade different organic compounds [29,31,32]. Among the halogenated contaminants, the current research with bimetallic nanoparticles is mainly focused on chlorinated alkane/alkene and aromatic compounds. Studies of brominated contaminants are limited. Moreover, the debromination of PBDEs with nano bimetallic Ni/Fe particles has not yet been demonstrated. This study aimed to investigate the feasibility of using Ni/Fe bimetallic nanoparticles to debrominate BDE209. Some influence factors, such as Ni/Fe addition, Ni loading, and initial BDE209 concentration, were investigated. Long-term performance of Ni/Fe nanoparticles, production of Ni in the solution during the reaction was also included. The focus of the paper was the main way of BDE209 removal, reaction pathway and the debromination mechanism.

2. Materials and methods

2.1. Chemicals

A standard solution of BDE209 was purchased from Cambridge Isotope Laboratories (CIL, Andover, MA) and used to establish the standard curve. Chemical grade BDE209 (98%) was purchased from Aladdin (Shanghai,China) and used as the degradation sample. Ferrous sulfate ($FeSO_4{\cdot}7H_2O$, >99%), nickel chloride ($NiCl_2{\cdot}6H_2O$, >99%), sodium borohydride ($NaBH_4$, >98%), polyvinyl pyrrolidone (PVP K-30), and ethanol (99.7%) were supplied by Tianjin Damao Chemical Agent Company (Tianjin, China). Methanol (HPLC grade) was supplied by Tianjin Kermel Chemical Reagents Company (Tianjin, China).

2.2. Preparation of Ni/Fe nanoparticles

The monometallic and bimetallic nanoparticles were synthesized using the sodium borohydride ($NaBH_4$) reduction method. Briefly, deionized water was deoxygenated by purging with N_2 gas for 30 min before use. Then, 0.1 M $FeSO_4{\cdot}7H_2O$ was prepared in 100 mL ethanol/water (30/70, v/v). Appropriate PVP (nanoparticle/PVP, w/w = 1/1) was added into the $FeSO_4{\cdot}7H_2O$ solution by mechanical agitation to completely mix the solution. Under nitrogen protection and vigorous stirring, 0.3 M $NaBH_4$ solution was rapidly added to the $FeSO_4{\cdot}7H_2O$ solution. The solution was stirred for 5 min, and stirring was stopped when the mixture turned black. Subsequently, the black particles formed were magnetically separated. In order to remove the excess amount of $NaBH_4$, the nanoparticles were rinsed three times with deoxygenated water and ethanol. The reaction can be described by the following equation:

$$2Fe^{2+} + 2H_20 + BH_4{}^- \rightarrow 2Fe^0 + BO_2{}^- + 4H^- + 2H_2 \quad (1)$$

To get post-coated bimetallic nanoparticles, 50 mL ethanol solution was added into the flask to redisperse the freshly prepared nanoscale Fe. Then, a specified amount of $NiCl_2{\cdot}6H_2O$ in 50 mL ethanol solution was added into the flask. The mixture was stirred for 30 min. The process is represented by the following equation:

$$Fe(s) + Ni^{2+} \rightarrow Fe^{2+} + Ni(s) \quad (2)$$

Separation and washing was similar to NZVI. Finally, the bimetallic nanoparticles were dried in a vacuum overnight at 50 °C before use.

Nanoscale Ni^0 was prepared from chemicals ($NiCl_2$) using the same method as preparing for NZVI. Meanwhile, in order to study the effect of PVP on degradation efficiency, the Ni/Fe nanoparticles without PVP were also prepared as the same method.

2.3. Characterization of nanoscale particles

Brunnaer–Emmett–Teller (BET) surface area analysis of Ni/Fe bimetallic nanoparticles was performed using an ASAP2020M surface analyzer (Micromeritics Instrument, USA) and by employing a nitrogen adsorption method.

The size and morphology of the Ni/Fe bimetallic nanoparticles were characterized with transmission electron microscopy (TEM, H-3000, Hitachi, Japan). After dispersion by an ultrasonator, several droplets of the nanoparticles/ethanol solution were deposited on a carbon-coated Cu-grid. After the ethanol completely evaporated, the samples were introduced into a vacuum chamber.

The crystalline phase of Ni/Fe bimetallic nanoparticles was determined using an X-ray diffractometer (Y – 2000, Dandong, China) with a Cu Kα radiation. The accelerating voltage and applied current were 30 kV and 20 mA, respectively.

X-ray photoelectron spectroscopy (XPS) was carried out on a ESCALAB 250 instrument (Thermo-VG Scientific, USA) using Al Kα radiation (photo energy 1486.6 eV) at pass energy of 150 eV. C1s spectra have been used as a reference with binding energy value of 284.8 eV. Element composition of Ni/Fe nanoparticles was also determined by EDS (HORIBA EMAX, Japan).

The Fe and Ni metal content of the bimetallic nanoparticles was determined by a flame atomic absorption spectrometer (TAS-986, Pgeneral, China)

2.4. Experimental procedures

2.4.1. Preparation of the BDE209 solution

It is well know that BDE209 with high hydrophobicity is practically difficultly soluble in water. In order to verify the feasibility of using new method to remove the BDE209 from solution, many researchers chose organic solvent (e.g. THF [33], methane [18], and acetonitrile [20]) as a solvent in their experiments. Meanwhile, for the purpose of our paper and the reaction of nano Ni/Fe must take place in the presence of water, so that we combined THF with an amount of water. Through many tests earlier, we found that when the THF increased to 60% in the solvent, dissolved different quantity of BDE209 (mg/L, 2 mg/L, 3 mg/L, and 4 mg/L) in the solvent become optimal. Therefore, the stock solution (100 mg/L) of BDE209 was made by using tetrahydrofuran (THF) as solvent. And a BDE209 simulated solution with the desired concentration was prepared by spiking a known volume of the stock solution into a certain proportion of THF/water solution.

2.4.2. Batch experimental procedure

Each batch reaction took place in a three-necked flask, which was placed in the dark at room temperature (28 ± 2 °C). The stirring rate was 200 rpm. For each time interval, small aliquots (1 mL for HPLC analysis or 5 mL for GC–MS) were taken out by a glass syringe and then filtered through a piece of membrane filter with the pore size of 0.45 μm for further analysis. Control experiments without bimetallic nanoparticles were also analyzed.

2.4.3. Experiment of long term performance

Batch experiment reaction took place in a three-necked flask, the experiment conditions were: temperature, 28 ± 2 °C; initial pH, 6.09; initial BDE209 concentration, 2 mg/L; Ni/Fe dosages, 4 g/L; speed of stirring, 200 rpm. After every cycle (3 h), magnetic separation was used to separate solution and nanoparticles, and then all supernatant was taken out, leaving nanoparticles in three-neck flask. After that, 100 mL fresh 2 mg/L BDE209 solution was added, keeping degradation. The taken-out supernatant was filtrated by

0.45 μm filtration membrane, and the concentration of BDE209 was tested by HPLC.

2.4.4. Experiment of nickel ion leaching

Eleven 250 mL three-neck flasks were used in this experiment. In every three-neck flask, 0.4 g Ni/Fe nanoparticles (23.8 wt%) and 100 mL BDE209 solution were added. The experiment conditions were: temperature, 28 ± 2 °C; initial pH, 6.09; initial BDE209 concentration, 2 mg/L; Ni/Fe dosages, 4 g/L; speed of stirring, 200 rpm. Every 3 h, one three-neck flask was taken out and the solution was filtered by 0.45 μm filtration membrane. 1 mL hydrochloric acid (1 mol/L) was added into the filtered solution. Then the Ni content in the solution was analyzed by AAS.

2.5. Analysis methods

2.5.1. HPLC analysis

The concentration of BDE209 in the samples was determined by high performance liquid chromatography (HPLC, LC10A HPLC, Shimadzu, Japan) with a UV detector (SPD-10AV) at 240 nm. A Dikma C18 column (250 mm × 4.6 mm) was used. The mobile phase was 100% methanol delivered at 1.2 mL/min. The sample size was 20 μL. The quantification was done with a calibration curve of BDE209 standards.

2.5.2. Bromide ion analysis

The concentration of bromide ion in the samples was measured by a pH meter (PHS-3B, Leici, Shanghai, China) coupled with a bromide ion-selective electrode (pBr-1, Leici, Shanghai, China). A saturated calomel electrode (Yueci Shanghai China) was used as a reference electrode (type: 217, Salt bridge: saturated potassium chloride).

2.5.3. Product analysis

After filtering though a Millipore filter (pore size 0.45 μm) to remove the particles, 2.5 mL of aqueous solution was spiked with ^{13}C-PCB141, poured into a separating funnel, and extracted by dichloromethane (2.5 mL × 3). The extracts were concentrated to 1 mL, cleaned, and fractionated on a silica/alumina column, which was packed from the bottom to the top with anhydrous sodium sulfate (1 cm), neutral alumina (6 cm), neutral silica gel (2 cm), sodium hydroxide silica (5 cm), neutral silica gel (2 cm), sulfuric acid silica (8 cm), and anhydrous sodium sulfate (3 cm). The PBDEs mixture was eluted with 70 mL of hexane/methylene chloride (1/1, v/v). The final extracted volume was reduced to 20 μL under a gentle N_2 stream.

Sample analysis was performed with a Model 6890 gas chromatograph (GC) coupled with a Model 5975 mass spectrometer (MS) (Agilent, USA) using negative chemical ionization (NCI) in the selected ion monitoring (SIM) mode. A DB5-MS (20 m × 0.25 mm i.d., 0.1 μm film thickness) capillary column was used to determine PBDEs congeners. The column temperature was initially held at 90 °C for 2 min. It was increased to 220 °C at 50 °C/min and then to 310 °C at 3 °C/min, where it was held for 5 min. The temperature of the injection port was 250 °C. Manual injection of 1 μL samples was conducted at a splitless mode. Methane was used as the chemical ionization moderating gas and helium as the carrier gas at a flow rate of 1 mL/min. The ion source and interface temperatures were all set to 150 °C. Ion fragments m/z 79 and 81 were monitored for tri- to hepta-BDEs and for BDE-209. For surrogate standards, m/z 372 was monitored for ^{13}C-PCB 141. Quantification of tri- to hepta-BDEs and BDE-209 was carried out using the external calibration standard method.

2.5.4. Kinetic analysis

A pseudo-first-order kinetics model was applied for the description of reductive debromination of BDE209:

$$\frac{dC_{BDE209}}{dt} = -k_{obs}C_{BDE209} \quad (3)$$

where k_{obs} is the observed rate constant of pseudo-first-order reaction and C_{BDE209} represents the concentration of BDE209 at any sampling time. The rate constants could be obtained by regression of a natural log of BDE209 concentration with respect to reaction time, according to the following equation:

$$\mathrm{Ln}\frac{C_{BDE209}}{C_{0BDE209}} = -k_{obs}t \quad (4)$$

where $C_{0BDE209}$ is the initial concentration of BDE209.

The half-life is calculated using the following equation:

$$t_{1/2} = \ln\frac{2}{k} = \frac{0.6931}{k} \quad (5)$$

3. Results and discussion

3.1. Characterization of nanoscale particles

The morphology and structure of both the Fe and Ni/Fe nanoparticles are shown in Fig. 1. The diameters of the synthesized nanoscale particles were lower than 100 nm. The TEM image of Fe nanoparticles exhibited an average particle diameter of approximately 50–80 nm, and the average diameter of the Ni/Fe nanoparticles was about 20–50 nm. These particles tended to aggregate together to form chain structures, which might have resulted from the magnetic interaction between small particles. The BET surface area of the Ni/Fe nanoparticles was 68 m^2/g, larger than that of nanoscale Fe (BET surface area was 35 m^2/g). The XRD pattern of the synthesized nanoparticles is shown in Fig. 1(c). The apparent peak at the 2θ of 44.9° indicated the presence of ZVI in both nanoparticles. However, the X-ray diffractometer did not detect the presence of Ni in the nanoparticles.

Therefore, XPS and EDS were further introduced to study the surface chemical compositions of Ni/Fe nanoparticles. As shown in Fig. 2, XPS and EDS analyses revealed that Fe, Ni, C and O were present on the surface of Ni/Fe. Moreover, in spectrum of Fe 2p (Fig. 3(a)), peak at 706.9 eV demonstrated the existence of NZVI, while broad peaks at 710.8 eV was attributed to iron oxides (α-Fe_2O_3). And in the spectrum of Ni 2p (Fig. 3(b)), the appearance of two peak, 855.8 eV and 852.3 eV were corresponding to Ni^{2+} and Ni^0. It is clearly demonstrated that the Fe and Ni with different valent existed on the surface of Ni/Fe nanoparticles. And the Ni in oxide form may be the reason why the surface area increased after nickel deposition.

3.2. Debromination of BDE209

3.2.1. Effect of PVP on debromination efficiency

It is well know that the nano particles can be easily agglomerated for the physical and chemical properties of nano iron particles, resulting in its poor performance in removal of environmental contaminants. In the process of preparation of NZVI particles, different dispersant agents were usually added so as to disperse the nano iron particles [34]. As a low-toxicity and low cost dispersant agent and stabilizer, polyvinlpnolidone with good solubility and stability can change the charge distribution of the surface and then generating the effect of electrostatic stabilizing, space steric and electrostatic space steric stabilizing, prevents aggregation of nanoparticles [35]. There is also a number of reports on the use of polyvinylpnolidone as dispersant agent in nano particles preparation [36–38]. In order to investigate the effect of PVP on catalytic activity, we compared

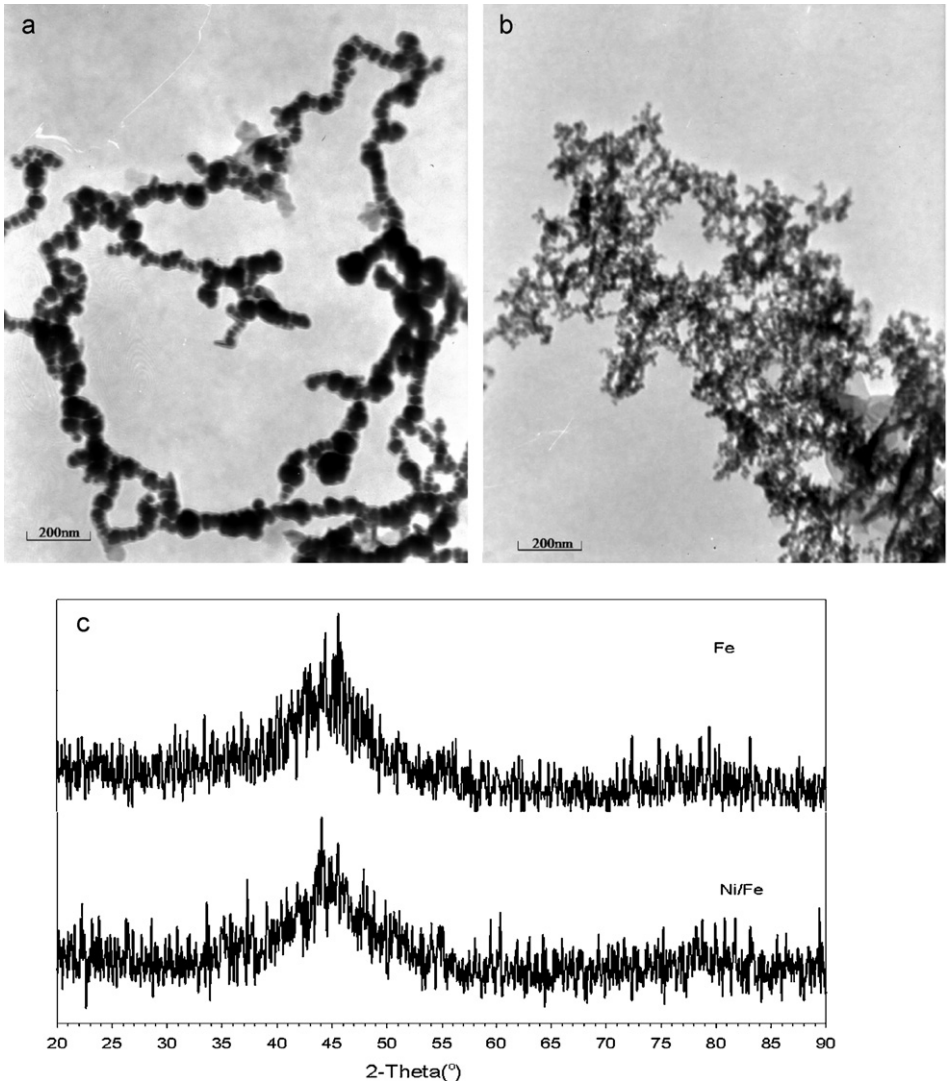

Fig. 1. Characterization of nanoparticles (Ni loading, 15.6 wt%): (a) TEM image of Fe nanoparticles; (b) TEM image of Ni/Fe bimetallic nanoparticles; (c) XRD pattern of Ni/Fe and Fe particles.

the degradation rate of BDE209 by Ni/Fe nanoparticles with and without PVP.

As shown in the Fig. 4, it is clearly shown that the degradation effectively of BDE209 by Ni/Fe nanoparticles with PVP was obvious quicker than the Ni/Fe without PVP. At the end of reaction time, near 100% of BDE209 have been removed by the PVP-Ni/Fe, but 65.48% for the Ni/Fe in absence of PVP. Degradation of contaminants by Fe^0-based particles is a surface-mediated process, increasing the surface area of nanoparticles will increase the degradation rate [26,30]. However, in the absence of an effective stabilizer, iron nanoparticles aggregate rapidly (in a few minutes) in water, resulting in micro-, millimeter-scale or even larger aggregates [39], so

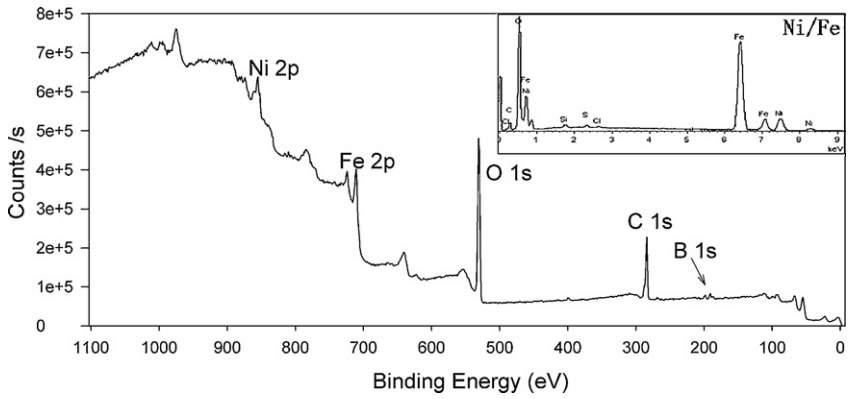

Fig. 2. XPS and EDS (inset) spectra of Ni/Fe nanoparticles (Ni loading, 15.6 wt%).

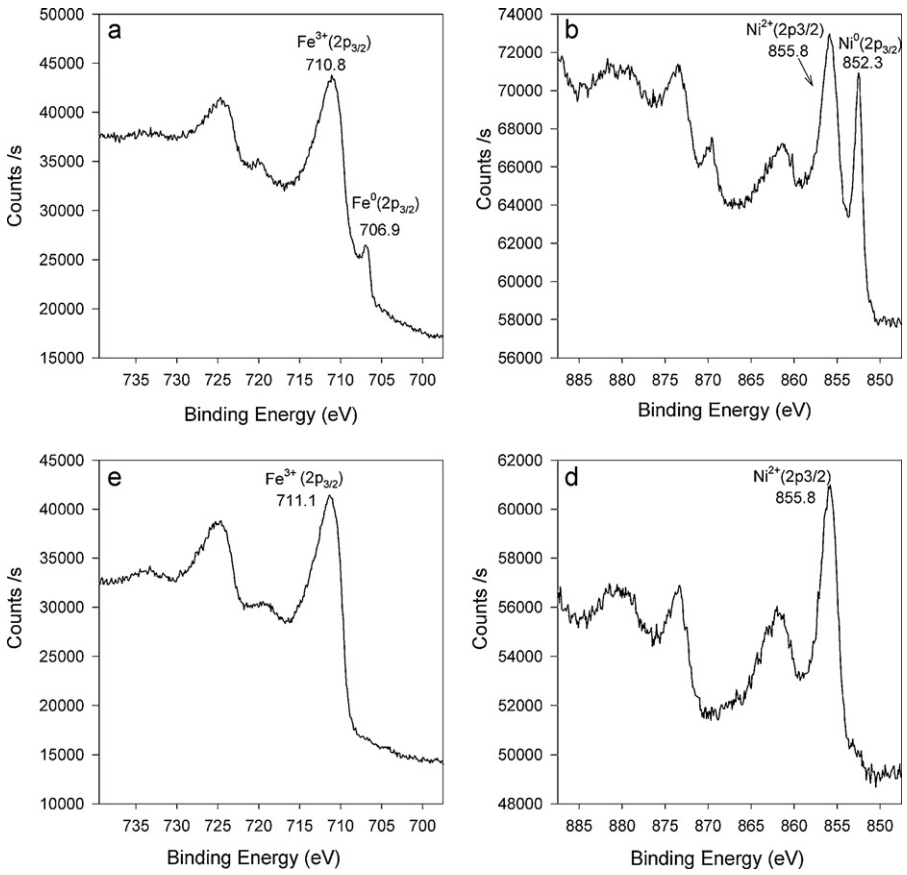

Fig. 3. XPS spectrum for the narrow scan of Fe 2p and Ni 2p on the surface of Ni/Fe (Ni loading, 15.6 wt%). (a) Narrow scan of Fe 2p before reaction; (b) narrow scan of Ni 2p before reaction; (c) narrow scan of Fe 2p after reaction; (d) narrow scan of Ni 2p after reaction.

that the reactivity of nanoparticles without stabilizer will decrease. Considering the effectiveness of PVP on debromination efficiency, Ni/Fe nanoparticles in the following experiments were all prepared with PVP.

3.2.2. *Effect of Ni/Fe bimetallic nanoparticles addition on debromination efficiency*

Based on Fig. 5, the removal efficiency varied with the amount of added Ni/Fe nanoparticles (0.5, 1, 2, 3, and 4 g/L). The removal percentage of BDE209 increased from 44.76% to 99% after 180 min of reaction when the amount of Ni/Fe nanoparticles increased from 0.5 g/L to 4 g/L. The degradation of BDE209 followed a pseudo-first-order kinetics. In light of previously published data [32,40], the removal efficiency or first-order rate constants could increase with increasing metal addition. Since the degradation of BDE209 occurred at the surface of the nanoparticles, an increase of the Ni/Fe nanoparticle concentration could simultaneously increase the number of active sites and reactive surface areas, leading to enhanced BDE209 degradation. Moreover, the BDE209 removal percentages by Ni/Fe nanoparticles increased rapidly within the first 90 min. This may be because the reduction of contaminations in the Ni/Fe nanoparticle system is a heterogeneous reaction which involves the adsorption of BDE209 on the Ni surface and the subsequent surface reaction [31]. Thus, the concentration of BDE209 in the liquid remarkably decreased in the beginning. However, the rate of BDE209 became slower after 90 min reaction due to the formation of surface passivation layers, this can determined by the spectrums of Ni/Fe nanoparticles before and after reaction (Fig. 3). Before reaction, in Fe 2p graph (Fig. 3(a)) the binding energies 706.9 eV and 710.8 eV, respectively, correspond to zero-valnet iron and iron oxide, while Ni 2p graph (Fig. 3(b)) at this time also shows that there are also two different states of Ni on the surface of nanometer metal, namely zero valence state (852.3 eV) and bivalence state (855.8 eV). However, after degradation reaction, the disappeared binding energies of zero valence state and the existence of ferric oxide's binding energies in the graphs of Fe 2p and Ni 2p (Fig. 3(c) and (d)) clearly shown that the formation of passivation on the surface. This passivation may inhibit the BDE209 reacted with Ni/Fe nanoparticles. So, the removal rate slow down.

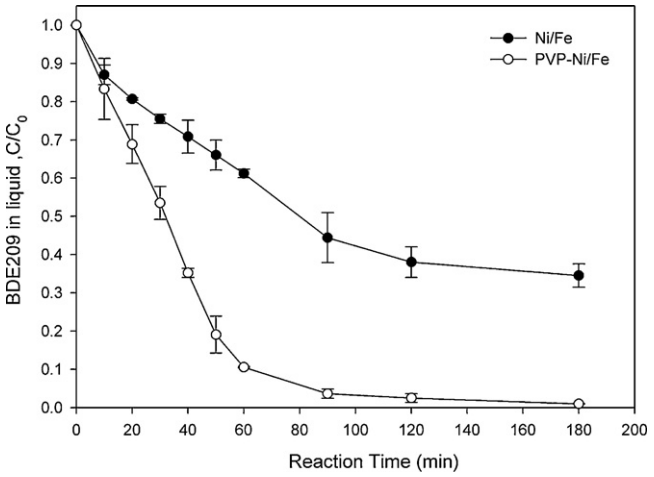

Fig. 4. Effect of PVP on the debromination efficiency. (Ni loading, 15.6 wt%; Ni/Fe addition, 4 g/L; initial concentration of BDE209, 2 mg/L, reaction time, 180 min, temperature, 28 ± 2° C; and pH 6.09).

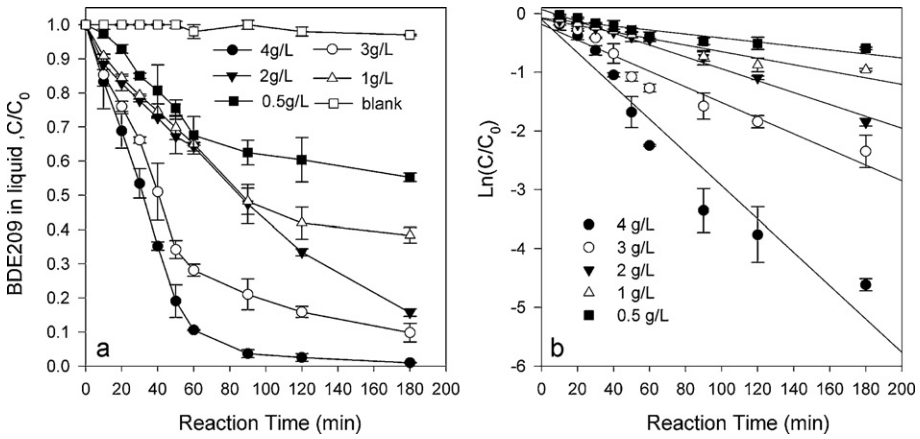

Fig. 5. (a) Effect of Ni/Fe addition on the debromination efficiency; (b) Relationship between the logarithmic plots of the BDE209 concentration versus time with different Ni/Fe additions (Ni loading, 15.6 wt%; initial concentration of BDE209, 1 mg/L; reaction time, 180 min; temperature, 28 ± 2° C; and pH 6.09).

The unit removal capacity (URC, i.e., amount of BDE209 removed versus Ni/Fe weight) decreased from 11.05 mg/g to 2.46 mg/g when the Ni/Fe dosage increased from 0.5 g/L to 4 g/L (Fig. 6). This is because, although the increased amount of Ni/Fe dosage could enhance the removal percentage, the higher addition did not take full advantage of surface areas of unit particles, resulted in URC declined.

3.2.3. Effect of initial BDE209 concentration on debromination efficiency

Four different concentrations of BDE209 (0.5, 1, 2, and 4 mg/L) were studied at a fixed Ni/Fe addition (4 g/L). From the data, the BDE209 is almost completely degraded within 180 min at different initial concentrations. Fig. 7(b) indicates that the degradation rate constant decreased with the increasing initial concentrations during the reaction time. For instance, at BDE209 concentration of 0.5 mg/L, the k_{obs} value was 0.084/min. In contrast, when the BDE209 concentration increased to 4 mg/L, the k_{obs} reduced to 0.023/min. The degradation of BDE209 in the Ni/Fe nanoscale particles system is a heterogeneous reaction, which involves adsorption of the BDE209 on the Ni surface and the subsequent surface reaction. Increasing the initial concentration of BDE209 would lead to competitive adsorption among the BDE209 molecules when adsorption reaction area of Ni/Fe is fixed. This would decrease the number of BDE209 molecules adsorbed and reduced on the Ni/Fe surface, leading to a decrease in the degradation efficiency.

In addition, the URC remarkably increased from 1.25 mg/g to 9.84 mg/g when the initial concentration increased from 0.5 mg/L to 4 mg/L (Fig. 8). The possible reason is that active sites of nano scale particles were lost due to formation of hydroxides and oxides on the surface while the reaction was progressing. The stoichiometric excess amounts of Ni/Fe would provide the necessary surface area for reaction. At a fixed concentration of Ni/Fe, the more initial concentration of BDE209, the more effective area can be used.

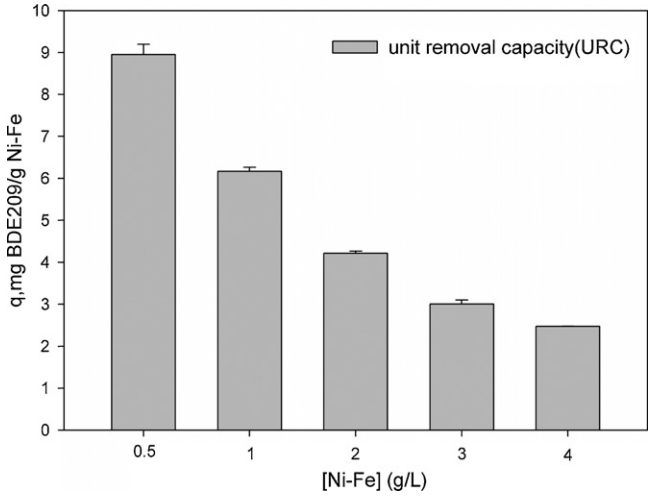

Fig. 6. Unit removal capacities (URC) versus Ni/Fe dosage (Ni loading, 15.6 wt%; initial concentration of BDE209, 1 mg/L; reaction time, 180 min; temperature, 28 ± 2° C; and pH 6.09).

3.2.4. Effect of Ni loading on debromination efficiency

Nickel is an excellent catalyst for hydrogenolysis [32,41]. As such, the addition of Ni to Fe nanoparticles can be very effective in accelerating dehalogenation. Therefore, the Ni content in the Ni/Fe particles may be an important factor in influencing dehalogenation efficiency.

Based on Fig. 9(a), BDE209 was slowly removed by Fe nanoparticles within a test period of 3 h. In contrast, the degradation rate of BDE209 by Ni/Fe (15.6/84.4, w/w) nanoparticles was about 93.4% within 90 min. The addition of a hydrogenation catalyst, such as Ni, had a tremendous effect on the dehalogenation rate. This has also been observed in the Ni/Fe nanoparticle system for reductive degradation of trichloroethylene (TCE) [42]. In addition, the efficiencies of degradation of BDE209 increased as the Ni loadings increased from 5 wt% to 30.9 wt%. The BDE209 removal percentage increased from 60% to 95% within 60 min. The reaction rate constants (k_{obs}) under the four Ni loadings (5.0 wt%, 15.6 wt%, 23.8 wt%, and 30.9 wt%) were determined as 0.0217/min, 0.0277/min, 0.0542/min, and 0.0604/min, respectively. The k_{obs} became larger with increasing Ni content. Several studies have postulated [40,43] that the atomic hydrogen adsorbed on the reductant surface (H_{ads}) is responsible for the bimetallic reactivity and that the metals, such as Ni, on the nanoscale Fe particles surface serves as a collector of hydrogen gas that results from the corrosion of Fe. Thus, a higher amount of Ni leads to faster reaction.

However, when nano Fe and nano Ni reacted with BDE209 independently, the removal efficiency of the BDE209 was 10.35% and 3.46% after 3 h reaction. The results have clearly demonstrated that in absence of Ni as a catalyst for nano Fe, or in absence of nano Fe as an electron donor for nano Ni, the degradation of the BDE209 is ineffective and unsatisfied. And it also illustrated that Ni in the bimetal served as a catalyst in the degradation of BDE209 rather than the electron donor or reducing agent.

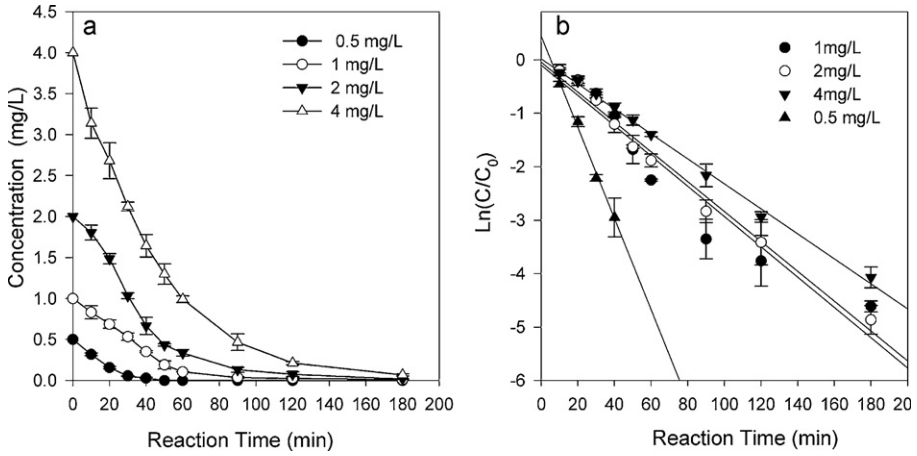

Fig. 7. (a) Effect of the initial concentration on the removal efficiency of BDE209; (b) Relationship between logarithmic plots of the BDE209 concentration versus time with different BDE209 concentrations (Ni/Fe addition, 4 g/L; Ni loading, 15.6 wt%; reaction time, 180 min; temperature, 28 ± 2° C; and pH 6.09).

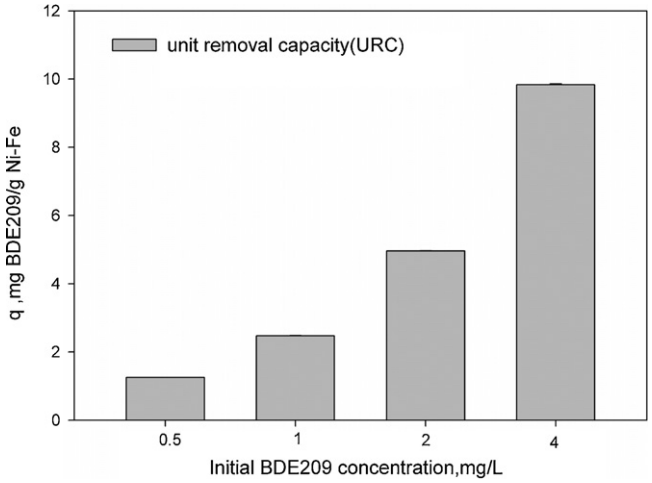

Fig. 8. Unit removal capacities (URC) versus initial BDE209 concentration (Ni/Fe addition, 4 g/L; Ni loading, 15.6 wt%; reaction time, 180 min; temperature, 28 ± 2° C; and pH 6.09).

Table 1
The mass balance of the BDE209 removal by Ni/Fe at different reaction time.

	30 min	60 min	180 min
BDE209 residual	0.103 mg	0.034 mg	0.002 mg
Adsorption on Ni/Fe	0.012 mg	0.008 mg	0.003 mg
Degradation	0.085 mg	0.158 mg	0.195 mg

3.3. Identify the main way of BDE209 removal

In order to investigate the main process for the BDE209 removal, the adsorbed BDE209 on the nanoparticles was carried out. As been seen from the Table 1, during 30 min reaction, the mass of residual BDE209 in the solution was 0.103 mg, while that adsorbed on the surface of particle was 0.012 mg. Based on the initial mass of BDE209 in the solution (0.2 mg), it can be got that the mass of degraded BDE209 was 0.085 mg, which was 7 times that of adsorption. When the reaction was 60 min, the mass of BDE209 in solution was 0.034 mg, and absorbed BDE209 was 0.008 mg, it meant that 0.158 mg BDE209 was degraded by Ni/Fe, 19 times that of adsorption. As the reaction reaches 180 min, the degraded BDE209 was 65 times that of adsorption. These results of mass balance indicated that the adsorption for the removal of BDE209 was less than that of degradation. Therefore we suggested that the principal way of BDE209 removal was degradation and debromination, but not adsorption.

3.4. Identification of the reaction products

Prior to application of Ni/Fe bimetallic nanoparticles for water treatment, it is critical to develop a better understanding of the

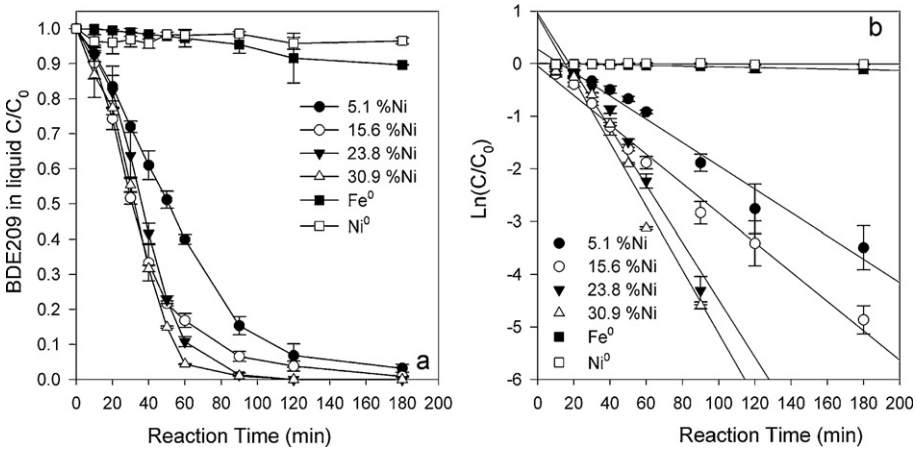

Fig. 9. (a) Effect of Ni loading on the removal efficiency of BDE209; (b) relationship between logarithmic plots of the BDE209 concentration versus time with different Ni loadings (Ni/Fe addition, 4 g/L; initial concentration of BDE209, 2 mg/L; reaction time, 180 min; temperature, 28 ± 2° C; and pH 6.09).

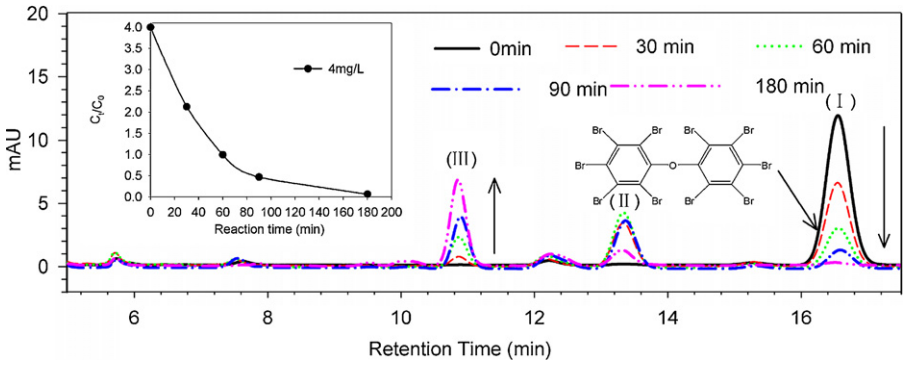

Fig. 10. HPLC chromatograms of BDE209 at different reaction times (Ni loading, 23.8 wt%; Ni/Fe addition, 4 g/L; initial concentration of BDE209, 2 mg/L, reaction time, 180 min, temperature, 28 ± 2° C; and pH 6.11).

degradation process and reaction pathways. To make sure the main reaction products of BDE209 removal by Ni/Fe nanoparticles, HPLC and GC/MS were used to monitor and identify the composition of the solution at different reaction times.

The HPLC chromatograms of the BDE209 solution at various reaction times are illustrated in Fig. 10. The amount of BDE209 (I), which was eluted at a retention time of 16.6 min, gradually decreased with increasing reaction time. Meanwhile, the amounts of intermediate product (II), which was eluted at a retention time of 13.4 min, and reaction products (III), which were eluted at a retention time of 10.8 min, varied with increasing reaction time. All the intermediate products were eluted from the chromatographic column before BDE209. The intermediate product (II) reached a maximum concentration at 60 mins and then decreased. However, these compounds were unidentified owing to the limitation of standard substances in HPLC. However, with reference to the reaction mechanism in the degradation of BDE209 by NZVI and Fe studied by Li et al. [44] and Keum and Li [24], we speculated that the new peaks that appeared during the reaction may be the lower PBDE congeners.

To confirm this, the degradation products in the solvent were identified by GC–MS (Fig. 11) .The identification was difficult because of a lack of enough PBDEs standards at the time of the experiment. There were some peaks with retention times that failed to match any of the 26 PBDEs standards (Supplementary data Table S2) in this experiment. Therefore, with the help of literature review on the analysis of degradation products [24,33,44] and the relative retention time database for DB-5 stationary phase [45], we speculated that several PBDEs congeners were the cause of this phenomenon.

Since the GC elution order [33,44] was well established, nona-BDEs could be identified exactly. In this experiment, BDE206 and BDE207 were identified by chemical standards. BDE208 was determined by its shorter retention time compared to BDE207. For octa-BDEs, two of five peaks appeared in the GC–MS chromatograms. The third and the fifth peaks were identified as BDE197 and BDE196, respectively, according to the retention time of the standards. The peak with a retention time slightly shorter than that of BDE197 was BDE204, and the peak with a retention time shorter than that of BDE196 was BDE203. This was concluded based on the relative retention times and orders of GC elution obtained from literature [33,44,45]. Moreover, Gerecke et al. [15] suggested that the earliest octa-BDE to be eluted on the commonly used non-polar GC columns was BDE202, owing to its lack of bromine at both para-positions. Wang et al. [44,45] also suggested that BDE202 elutes earlier than all other octa-BDEs, based on their Quantitative Structure Retention Relationships (QSRRs). For these reasons, we assumed that the first octa-BDE peak was BDE202. Several hepta-BDEs were observed in this work. Among them, BDE191, BDE184, and BDE183 were identified using chemical standards. The other major hepta-BDE peaks observed between BDE184 and BDE183, or BDE183 and 191, could not be confidently determined because of the lack of chemical standards. These unknown peaks might have been hepta-BDEs or other lower PBDEs that might be eluted at the same time [45]. In addition, some hexa-BDEs were formed, and four of them (BDE138, BDE153, BDE154, and BDE156) were identified confidently based on chemical standards. However, a major peak between BDE154 and 153 was hard to identify. Li et al. [44] speculated that this major peak may be coeluting hexa-BDE congeners. Four penta-BDEs were identified using chemical standards, and they were BDE-85, BDE-99, BDE-100, and BDE119. As the reaction progressed, some lower PBDEs appeared in this experiment. They were difficult to identify because of insufficient separation in the 20 m column, resulting in broad peaks in the chromatogram. By matching the retention time with the chemical standards and comparing the concentration at different reaction times, we determined that these were BDE47, which is commonly detected in the environment, and BDE66.

3.5. Degradation pathways

Based on the identification of the intermediates and the changes in the total mass spectrum, the degradation of BDE209 was determined to be a stepwise dehalogenation process. This speculation is the same as that of the degradation of organic halogen pollutants by nano Fe-based materials reported in several papers [30,46]. In the first step, a bromine ion was removed from deca-BDE through a reaction with Ni/Fe nanoparticles to form nona-BDEs. Then, three newly formed nona-BDEs were also transformed to lower PBDEs via reductive elimination. This phenomenon was reflected clearly by the increasing concentration of bromide ion in solution during the reaction time. As shown in the Fig. 12, at 30 min of the reaction, 48.5% BDE209 in the solution was removed, and the concentration of bromide ion in solution reaches 0.0369 mg/L. At 60 min of the reaction time, concentration of the removed BDE209 was 83%, and the concentration of bromide ions in the solution was 0.0647 mg/L. Furthermore, at 180 min, removal efficiency of BDE209 got near to 100%, while the concentration of bromide ion presents a more substantial rise. But this process continued until some products appeared which were difficult to reduce by Ni/Fe nanoparticles, or the products could not be supplied with reaction sites. In addition, mono- to tri-BDEs could possibly have appeared at the end of the experiment, but these could not be accurately identified. Therefore, the final products of this research were regarded as tetra-BDEs (mainly BDE-47). A simple degradation pathway of BDE 209 is described in Fig. 13. A more comprehensive analytical approach is needed to understand the details of the pathway.

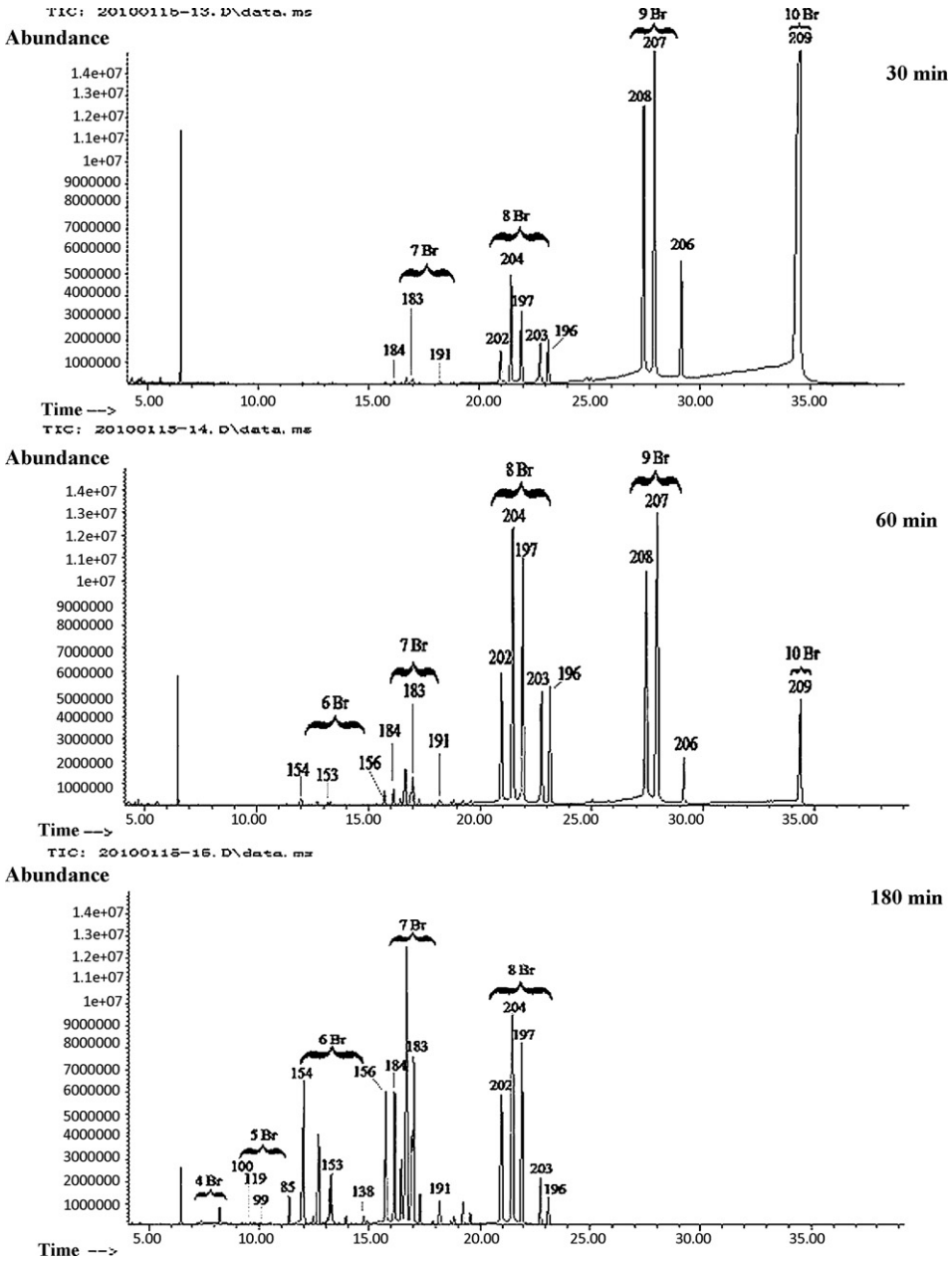

Fig. 11. GC–MS chromatogram of BDE209 at different reaction times (Ni loading was 23.8 wt%, Ni/Fe addition was 4 g/L, initial concentration of BDE209 was 2 mg/L, reaction time was 180 min, temperature at 28 ± 2° C, and pH 6.11).

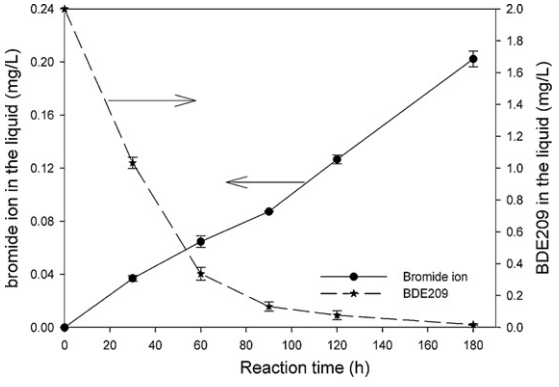

Fig. 12. BDE209 removal and bromide ion generation with reaction time. (Ni loading was 15.6 wt%, Ni/Fe addition was 4 g/L, initial concentration of BDE209 was 2 mg/L, reaction time was 180 min, temperature at 28 ± 2° C, and pH 6.09).

3.6. Degradation mechanism

In order to verify and demonstrate the main reason for the debromination process, the reactions were further studied under various solvent conditions, and the results are presented in Fig. 14. The proportion of water in the solvent was one of the important factors influencing debromination efficiency. Under the condition of pure tetrahydrofuran or a mixture of tetrahydrofuran and ethanol, none of the BDE209 was degraded within 180 min. However, when the amount of water in the solutions increased, the degradation of BDE209 was notably enhanced. From the experimental data, the removal percentage of BDE209 within 180 min reached near 100% using a solution with 40% water. However, it decreased to 64.82% and 17.32% when the proportion of water declined to 30% and 20%, respectively. For the reduction pathway and the experimental data discussed above, the main reason for the debromination process was catalytic hydrogenation, and the atomic hydrogen was the

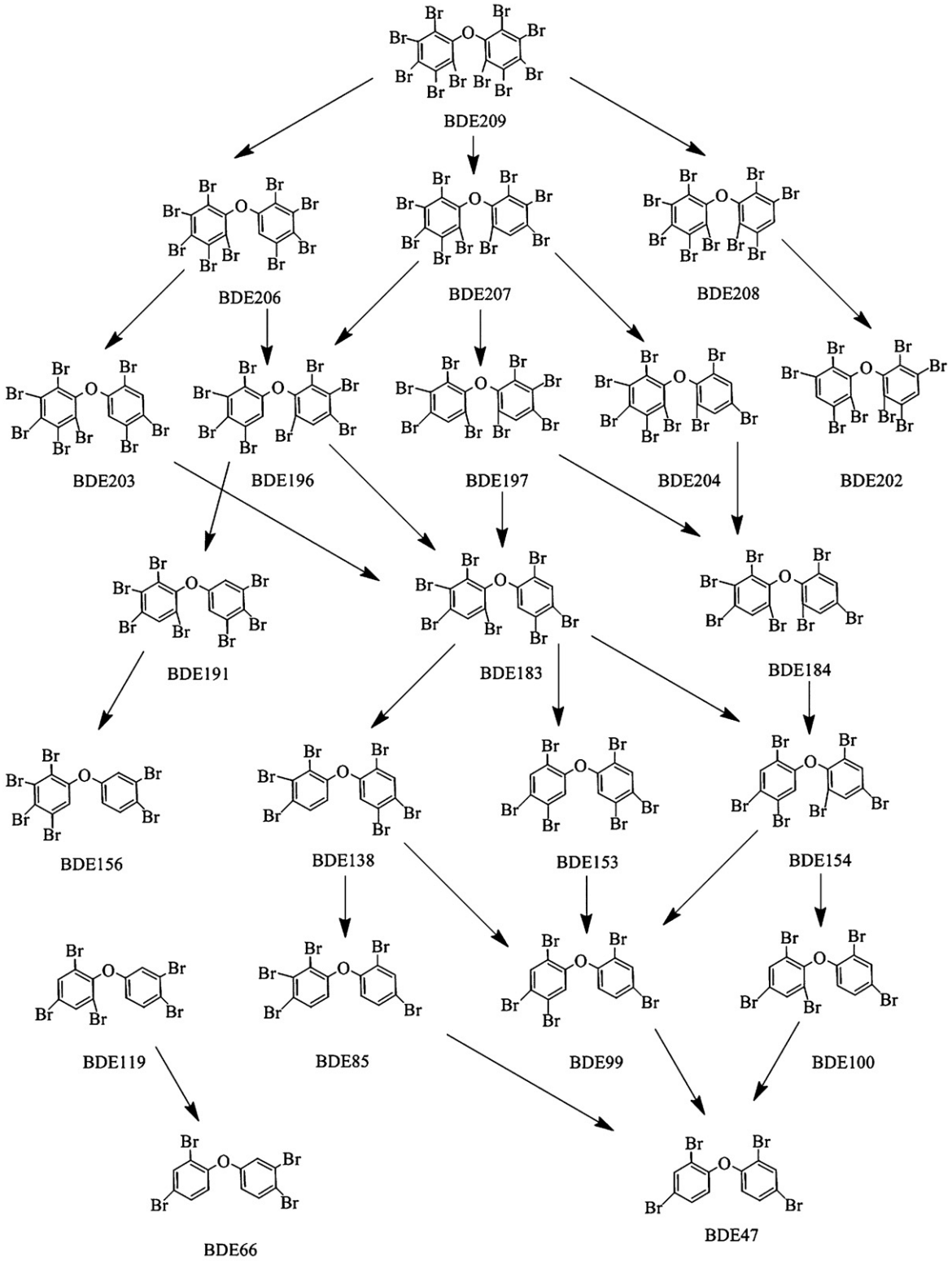

Fig. 13. Proposed pathway for the degradation of BDE209 by Ni/Fe nanoparticles.

main reducing agent. The steps of catalytic, reductive dehalogenation by Ni/Fe bimetallic particles could be depicted by Eqs. (6)–(10) [27,40]

$$(1)\ Fe^0 \rightarrow Fe^{2+} + 2e^- \quad (6)$$

$$(2)\ 2H^+ + 2e^- \rightarrow H_2(g) \quad (7)$$

$$(3)\ Ni + H_2 \rightarrow Ni{\cdot}2H* \quad (8)$$

$$(4)\ Ni + RBr_n \rightarrow Ni\cdots Br_n\cdots R \quad (9)$$

$$(5)\ Ni\cdots 2H^* + Ni\cdots Br_n\cdots R \rightarrow RBr_{n-1}H + H^+ + Br^- + 2Ni \quad (10)$$

The reactions above shown that the presence of hydrion in the solvent plays the most important role in degradation of the BDE209,

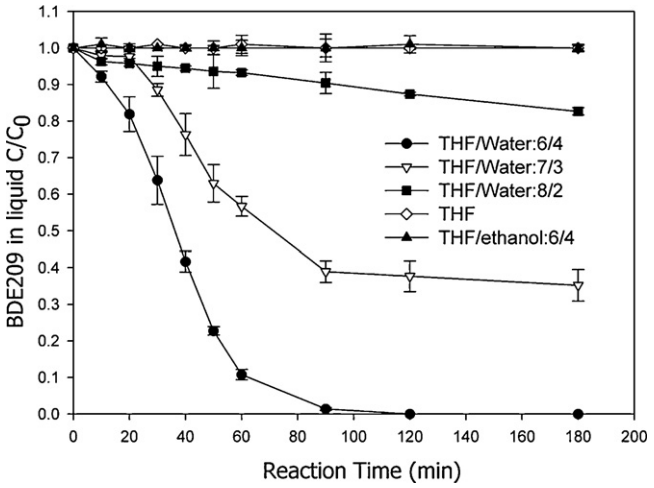

Fig. 14. Effect of solvent conditions on the BDE209 removal efficiency (Ni loading, 23.8 wt%; Ni/Fe addition, 4 g/L; initial concentration of BDE209, 2 mg/L; reaction time, 180 min; temperature, 28 ± 2° C).

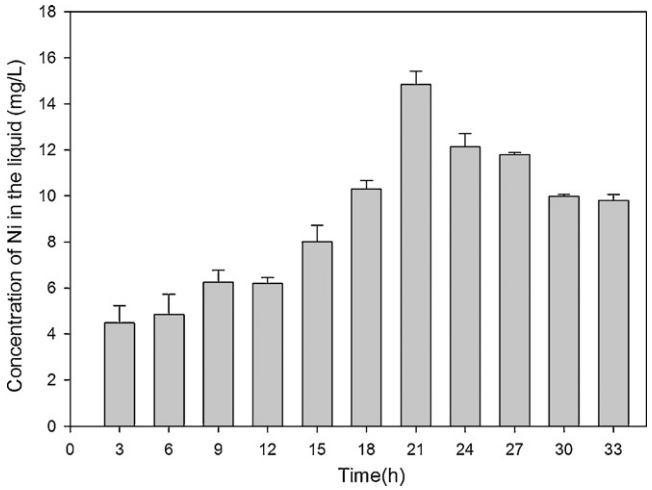

Fig. 16. Leaching of Ni in solution during degradation of BDE209. (Ni loading, 23.8 wt%; Ni/Fe addition, 4 g/L; initial concentration of BDE209, 2 mg/L; temperature, 28 ± 2° C, and pH 6.09).

and the ionization constants (K_a) of different solvents using in this paper followed this trend: water ($K_a = 1 \times 10^{-14}$) > ethanol ($K_a = 1 \times 10^{-30}$ > THF (aprotic solvent). This meant that the water can provide more hydrion than other organic solvents for the reduction. Consequently, in the presence of water, particularly at 20%, 30%, and 40% water contents, the reaction rate improved for increasing water content, as well as increasing the concentration of hydrion in the solvent. But in organic solvent system, THF is the aprotic solvent, and the system cannot provide hydrion for the reaction. Although ethanol is a protic solvent like water, its ionization constants (K_a) is 10^{16} times smaller than water's, so the solution could not provide enough protons for the reaction quickly, resulted in the reaction slowly, or even not occurring in the organic solvents.

3.7. Long term performance and leaching of Ni

3.7.1. Long term performance of Ni/Fe in degradation

Nano Ni/Fe's long-term performance of degradation of BDE 209 is shown in the Fig. 15. In the first six degradation cycles, it could be found that the removal rate by nano Ni/Fe was more than 90% for 2 mg/L BDE209. When the experiment was up to the seventh cycle, the degradation efficiency was down to 65.01%. From that, the removal effect of nano Ni/Fe gradually decreased. To the tenth degradation cycle, only 9.04% of 2 mg/L BDE209 was removed in 3 h. Therefore, the effective degradation cycle of nanoscale Ni/Fe particles was six times. But in practical engineering application, Ni/Fe can be modified in different ways (e.g. Membranes [34]) to improve its service life.

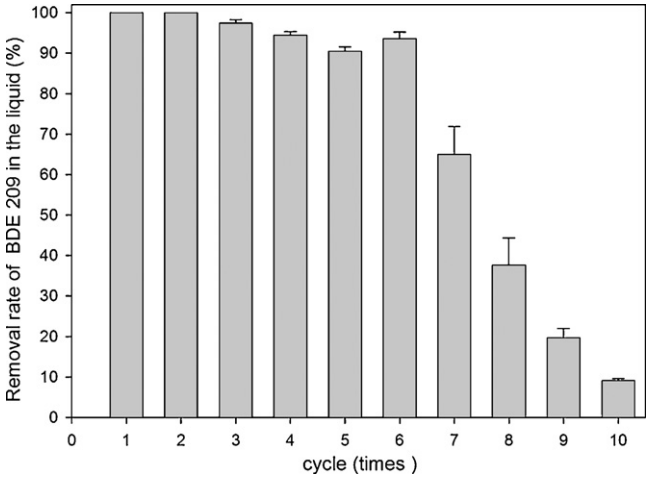

Fig. 15. Stability and durability of Ni/Fe nanoparticles in BDE 209 degradation. (Ni loading, 23.8 wt%; Ni/Fe addition, 4 g/L; initial concentration of BDE209, 2 mg/L; temperature, 28 ± 2° C, and pH 6.09).

3.7.2. Leaching of Ni

As shown in the Fig. 16, when the reaction time was increased from 3 h to 21 h, the Ni ion content in the solution increased from 4.48 mg/L to 14.83 mg/L. And then, when the reaction time extended longer than 21 h, the Ni ion content in the solution started to decrease and then tended to be balanced. At the 33 h, Ni ion content in the solution was 9.81 mg/L. This concentration of Ni ion exceeded the highest limit content of nickel in sewage (1 mg/L) which was regulated in China's national comprehensive discharge standard of sewage (GB8978-1996). Therefore, in practical application, it is necessary to add appropriate follow-up processing steps for avoiding the nickel of dissolution.

4. Conclusions

This paper investigated the degradation of BDE209 by synthesized Ni/Fe bimetallic nanoparticles. The debromination of BDE209 by Ni/Fe bimetallic nanoparticles was effective and feasible at ambient temperature and pressure, and the removal efficiency was significantly faster than NZVI under the same conditions. The addition of Ni to Fe nanoparticles enhanced the dehalogenation efficiency. The degradation of BDE209 by Ni/Fe followed a pseudo-first-order kinetics, which can be described by the formula: $\mathrm{Ln}(C_t/C_0) = -k_{obs}t$. The removal rate constant k_{obs} was proportional to the Ni/Fe nanoparticle dosage and Ni loading. It was inversely proportional to the BED209 initial concentration. Based on the results of surface adsorption of BDE209, the main way of BDE209 removal was degradation. And the bromide ion analysis, HPLC and GC–MS analysis deduced that the hydrodebromination played a leading role in the reaction. Through the reduction of BDE209 in different solvent condition, it was strongly recommend that hydrion was the driving forces of reaction. Finally, the experiment of long term performance and leaching of Ni shown that bimetallic nanoscale particles had the ability to remain active for 6 cycles, and 14.83 mg/L were detected in the solution after 21 h reaction.

Acknowledgments

The authors are grateful for the financial support provided by the National Science and Technology Major Projects of Water Pollution Control and Management of China (2009ZX07011).

Appendix A. Supplementary data

Supplementary data associated with this article can be found, in the online version, at doi:10.1016/j.jhazmat.2010.09.113.

References

[1] Y. Luo, X.J. Luo, Z. Lin, Polybrominated diphenyl ethers in road and farmland soils from an e-waste recycling region in Southern China: concentrations, source profiles, and potential dispersion and deposition, Sci. Total. Environ. 407 (2009) 1105–1113.
[2] X.Z. Peng, C.M. Tang, Y.Y. Yu, J.H. Tan, Q.X. Huang, J.P. Wu, S.J. Chen, B.X. Mai, Concentrations, transport, fate, and releases of polybrominated diphenyl ethers in sewage treatment plants in the Pearl River Delta, South China, Environ. Int. 35 (2009) 303–309.
[3] X.J. Luo, J. Liu, Y. Luo, X.L. Zhang, J.P. Wu, Z. Lin, S.J. Chen, B.X. Mai, Z.Y. Yang, Polybrominated diphenyl ethers (PBDEs) in free-range domestic fowl from an e-waste recycling site in South China: Levels, profile and human dietary exposure, Environ. Int. 35 (2009) 253–258.
[4] T. Shi, S.J. Chen, X.J. Luo, X.L. Zhang, C.M. Tang, Y. Luo, Y.J. Ma, J.P. Wu, X.Z. Peng, B.X. Mai, Occurrence of brominated flame retardants other than polybrominated diphenyl ethers in environmental and biota samples from southern China, Chemosphere 74 (2009) 910–916.
[5] X.J. Luo, M. Yu, B.X. Mai, S.J. Chen, Distribution and partition of polybrominated diphenyl ethers (PBDEs) in water of the Zhujiang River Estuary, Chin. Sci. Bull. 53 (2008) 493–500.
[6] Q. Luo, M.H. Wong, Z.W. Cai, Determination of polybrominated diphenyl ethers in freshwater fishes from a river polluted by e-wastes, Talanta 72 (2007) 1644–1649.
[7] M. TA, A perspective on the potential health risks of PBDEs, Chemosphere 46 (2002) 745–755.
[8] K. Jakobsson, K. Thuresson, L. Rylander, A. Sjödin, L. Hagmar, A. Bergman, Exposure to polybrominated diphenyl ethers and tetrabromobisphenol A among computer technicians, Chemosphere 46 (2002) 709–716.
[9] E. Mariussen, E. Fjeld, K. Breivik, E. Steinnes, A. Borgen, G. Kjellberg, M. Schlabach, Elevated levels of polybrominated diphenyl ethers (PBDEs) in fish from Lake Mjosa, Norway, Sci. Total. Environ. 390 (2008) 132–141.
[10] B.J. Restrepo, K. Kannan, D.P. Rapaport, B.D. Rodan, Polybrominated diphenyl ethers and polychlorinated biphenyls in human adipose tissue from New York, Environ. Sci. Technol. 39 (2005) 5177–5182.
[11] A. Sjödin, R.S. Jones, J.F. Focant, C. Lapeza, R.Y. Wang, E.E. McGahee III, Y. Zhang, W.E. Turner, B. Slazyk, L.L. Needham, D.G. Patterson, Retrospective time-trend study of polybrominated diphenyl ether and polybrominated and polychlorinated biphenyl levels in human serum from the United States, Environ. Health Persp. 112 (2004) 654–658.
[12] P. Lindberg, U. Sellstrom, L. Haggberg, C.A. de Wit, Higher brominated diphenyl ethers and hexabromocyclododecane found in eggs of peregrine falcons (Falco peregrinus) breeding in Sweden, Environ. Sci. Technol. 38 (2004) 93–96.
[13] P.A. Behnisch, K. Hosoe, S. Sakai, Brominated dioxin-like compounds: in vitro assessment in comparison to classical dioxin-like compounds and other polyaromatic compounds, Environ. Int. 29 (2003) 861–877.
[14] Agency for Toxic Substances and Disease Registry Division of Toxicology and Environmental Medicine, Public health statement for polybrominated diphenyl ethers (PBDEs), Atlanta, 2004.
[15] A.C. Gerecke, P.C. Hartmann, N.V. Heeb, H.E. Kohler, W. Giger, P. Schmid, M. Zennegg, M. Kohler, Anaerobic degradation of decabromodiphenyl ether, Environ. Sci. Technol. 39 (2005) 1078–1083.
[16] J.Z. He, K.R. Robrock, L. Alvarez-Cohen, Microbial reductive debromination of polybrominated diphenyl ethers (PBDEs), Environ. Sci. Technol. 40 (2006) 4429–4434.
[17] K.R. Robrock, P. Korytár, L. Alvarez-Cohen, Pathways for the anaerobic microbial debromination of polybrominated diphenyl ethers, Environ. Sci. Technol. 42 (2008) 2845–2852.
[18] J. Eriksson, N. Green, G. Marsh, A. Bergman, Photochemical decomposition of 15 polybrominated diphenyl ether congeners in methanol/water, Environ. Sci. Technol. 38 (2004) 3119–3125.
[19] G. Soderstrom, U. Sellstrom, C.A. de Wit, M. Tysklind, Photolytic debromination of decabromodiphenyl ether (BDE 209), Environ. Sci. Technol. 38 (2004) 127–132.
[20] C.Y. Sun, D. Zhao, C.C. Chen, W.H. Ma, J.C. Zhao, TiO2-mediated photocatalytic debromination of decabromodiphenyl ether: kinetics and intermediates, Environ. Sci. Technol. 43 (2009) 157–162.
[21] D.M. Chen, D. Yang, Q. Wang, Z.G. Jiang, Effects of boron doping on photocatalytic activity and microstructure of titanium dioxide nanoparticles, Ind. Eng. Chem. Res. 45 (2006) 4110–4116.
[22] C.B. Wang, W.X. Zhang, Synthesizing nanoscale iron particles for rapid and complete dechlorination of TCE and PCBs, Environ. Sci. Technol. 31 (1997) 2154–2156.
[23] G.V. Lowry, K.M. Johnson, Congener-specific dechlorination of dissolved PCBs by microscale and nanoscale zerovalent iron in a water/methanol solution, Environ. Sci. Technol. 38 (2004) 5208–5216.
[24] Y. Keum, Q.X. Li, Reductive debromination of polybrominated diphenyl ethers by zerovalent iron, Environ. Sci. Technol. 39 (2005) 2280–2286.
[25] H. Choi, S.R. Al-Abed, S. Agarwal, D.D. Dionysiou, Synthesis of reactive nano-Fe/Pd bimetallic system-impregnated activated carbon for the simultaneous adsorption and dechlorination of PCBs, Chem. Mater. 20 (2008) 3649–3655.
[26] L. Li, M.H. Fan, R. Brown, J.H. Van Leeuwen, J.J. Wang, W.H. Wang, Y.H. Song, P.Y. Zhang, Synthesis, properties, and environmental applications of nanoscale iron-based materials: a review, Crit. Rev. Environ. Sci. Technol. 36 (2006) 405–431.
[27] X.H. Qiu, Z.Q. Fang, Degradation of halogenated organic compounds by modified nano zero-valent iron, Prog. Chem. 22 (2010) 291–297.
[28] J. Kim, P.G. Tratnyek, Y. Chang, Rapid dechlorination of polychlorinated dibenzo-p-dioxins by bimetallic and nanosized zerovalent iron, Environ. Sci. Technol. 42 (2008) 4106–4112.
[29] X.Y. Wang, C. Chen, H.L. Liu, J. Ma, Characterization and evaluation of catalytic dechlorination activity of Pd/Fe bimetallic nanoparticles, Ind. Eng. Chem. Res. 47 (2008) 8645–8651.
[30] T.T. Lim, J. Feng, B.W. Zhu, Kinetic and mechanistic examinations of reductive transformation pathways of brominated methanes with nano-scale Fe and Ni/Fe particles, Water Res. 41 (2006) 875–883.
[31] A.D. Bokare, R.C. Chikate, C.V. Rode, K.M. Paknikar, Iron-nickel bimetallic nanoparticles for reductive degradation of azo dye orange G in aqueous solution, Appl. Catal. B Environ. 79 (2008) 270–278.
[32] X. Wang, C. Chen, Y. Chang, H. Liu, Dechlorination of chlorinated methanes by Pd/Fe bimetallic nanoparticles, J. Hazard. Mater. 161 (2009) 815–823.
[33] H.X. Zhao, F.F. Zhang, B.C. Qu, X.Y. Xue, X.M. Liang, Wet air co-oxidation of decabromodiphenyl ether (BDE209) and tetrahydrofuran, J. Hazard. Mater. 169 (2009) 1146–1149.
[34] G.K. Parshetti, R. Doong, Dechlorination of trichloroethylene by Ni/Fe nanoparticles immobilized in PEG/PVDF and PEG/nylon 66 membranes, Water Res. 43 (2009) 3086–3094.
[35] S.M. Gao, X.D. Wang, L. Lian, S. Luo, X. Zhao, S.S. Liu, L.S. Wang, Preparation of nano zero-valent iron particles by modified liquid phase reduction method, J. Nanjing Univ. (Nat. Sci.) 43 (2007) 358–368.
[36] A. Nemamcha, J. Rehspringer, D. Khatmi, Synthesis of palladium nanoparticles by sonochemical reduction of palladium(II) nitrate in aqueous solution, J. Phys. Chem. B 110 (2006) 383–387.
[37] S. Choi, A.I. Gopalan, J. Ryu, K. Lee, Hollow spherical nanocapsules of poly(pyrrole) as a promising support for Pt/Ru nanoparticles based catalyst, Mater. Chem. Phys. 120 (2010) 18–22.
[38] T. Umegaki, J.M. Yan, X.B. Zhang, H. Shioyama, N. Kuriyama, Q. Xu, Preparation and catalysis of poly(N-vinyl-2-pyrrolidone) (PVP) stabilized nickel catalyst for hydrolytic dehydrogenation of ammonia borane, Int. J. Hydrogen Energy 34 (2009) 3816–3822.
[39] F. He, D.Y. Zhao, C. Paul, Field assessment of carboxymethyl cellulose stabilized iron nanoparticles for in situ destruction of chlorinated solvents in source zones, Water Res. 44 (2010) 2360–2370.
[40] X.Y. Wang, C. Chen, Y. Chang, H.L. Liu, Dechlorination of chlorinated methanes by Pd/Fe bimetallic nanoparticles, J. Hazard. Mater. 161 (2009) 815–823.
[41] C. Lee, D.L. Sedlak, C.H. Lee, D.L. Sedlak, Enhanced formation of oxidants from bimetallic nickel–iron nanoparticles in the presence of oxygen, Environ. Sci. Technol. 42 (2008) 8528–8533.
[42] B. Schrick, J.L. Blough, A.D. Jones, T.E. Mallouk, Hydrodechlorination of trichloroethylene to hydrocarbons using bimetallic nickel–iron nanoparticles, Chem. Mater. 14 (2002) 5140–5147.
[43] D.M. Cwiertny, S.J. Bransfield, A.L. Roberts, Influence of the oxidizing species on the reactivity of iron-based bimetallic reductants, Environ. Sci. Technol. 41 (2007) 3734–3740.
[44] A. Li, C. Tai, Z.S. Zhao, Y.W. Wang, Q.H. Zhang, G.B. Jiang, J.T. Hu, Debromination of decabrominated diphenyl ether by resin-bound iron nanoparticles, Environ. Sci. Technol. 41 (2007) 6841–6846.
[45] Y.W. Wang, A. Li, H.X. Liu, Q.G. Zhang, W.P. Ma, W.L. Song, G.B. Jiang, Development of quantitative structure gas chromatographic relative retention time models on seven stationary phases for 209 polybrominated diphenyl ether congeners, J. Chromatogr. A. 1103 (2006) 314–328.
[46] N. He, P.J. Li, Y.C. Zhou, W.X. Ren, S.X. Fan, V.A. Verkhozina, Catalytic dechlorination of polychlorinated biphenyls in soil by palladium-iron bimetallic catalyst, J. Hazard. Mater. 164 (2009) 126–132.